Directed evolution of the tryptophan synthase β-subunit for stand-alone function recapitulates allosteric activation

Andrew R. Buller[1], Sabine Brinkmann-Chen[1], David K. Romney, Michael Herger, Javier Murciano-Calles, and Frances H. Arnold[2]

Division of Chemistry and Chemical Engineering, California Institute of Technology, Pasadena, CA 91125

Enzymes in heteromeric, allosterically regulated complexes catalyze a rich array of chemical reactions. Separating the subunits of such complexes, however, often severely attenuates their catalytic activities, because they can no longer be activated by their protein partners. We used directed evolution to explore allosteric regulation as a source of latent catalytic potential using the β-subunit of tryptophan synthase from *Pyrococcus furiosus* (*Pf*TrpB). As part of its native αββα complex, TrpB efficiently produces tryptophan and tryptophan analogs; activity drops considerably when it is used as a stand-alone catalyst without the α-subunit. Kinetic, spectroscopic, and X-ray crystallographic data show that this lost activity can be recovered by mutations that reproduce the effects of complexation with the α-subunit. The engineered *Pf*TrpB is a powerful platform for production of Trp analogs and for further directed evolution to expand substrate and reaction scope.

protein engineering | allostery | noncanonical amino acid | PLP

Heteromeric enzyme complexes catalyzing a rich array of useful reactions are often allosterically regulated by their protein partners, such that the catalytic subunits are much less active when isolated (1–3). Utilization of isolated enzyme subunits, however, is desirable for biosynthetic applications, where expressing large complexes increases the metabolic load on the host cell and complicates efforts to engineer activity, substrate specificity, stability, and other properties. A solution to these problems is to engineer the isolated subunit to function independently. However, it is unknown to what extent mutations in the amino acid sequence can reproduce the complex structural and functional changes that are induced by binding of a partner protein.

Tryptophan synthase (TrpS; EC 4.2.1.20) is a heterodimeric complex that catalyzes the formation of L-tryptophan (Trp, **1**) from L-serine (Ser, **2**) and indole glycerol phosphate (IGP, **3**; Fig. 1A) (2). The mechanism of this transformation has been extensively studied for TrpS from *Escherichia coli* and *Salmonella typhimurium*, where it has been shown the enzyme consists of two subunits, TrpA (α-subunit) and TrpB (β-subunit), both of which have low catalytic efficiencies in isolation (4). The activities of both subunits increase upon complex formation and are further regulated by an intricate and well-studied allosteric mechanism (2). IGP binding to the α-subunit stimulates pyridoxal phosphate (PLP)-dependent aminoacrylate formation in the β-subunit [E(A-A); Fig. 1B], which in turn promotes retro-aldol cleavage of IGP in the α-subunit, releasing indole (4). This tightly choreographed mechanism serves to prevent the free diffusion of indole, which is only released from the α-subunit when the complex is in a closed conformation that forms a 25-Å tunnel through which indole diffuses into the β-subunit (5). Here, indole reacts with E(A-A) in a C–C bond-forming reaction, yielding L-tryptophan as product (Fig. 1B) (2, 5). These allosteric effects are mediated through the rigid-body motion of the communication (COMM) domain and a monovalent cation (MVC) binding site within the β-subunit (Fig. 1A), which undergo complex conformational transitions

associated with open, partially closed, and fully closed states during the catalytic cycle (2, 4, 6).

TrpS is a naturally promiscuous enzyme complex: the model system from *S. typhimurium* catalyzes its β-substitution reaction with most haloindoles, methylindoles, and aminoindoles, along with an assortment of nonindole nucleophiles for C–S, C–N, and C–C bond formation (7). Such noncanonical amino acids (NCAAs) have diverse applications in chemical biology (8), serve as intermediates in the synthesis of natural products (9, 10), and are privileged scaffolds for the development of pharmaceuticals (11). Despite its natural ability to produce these desirable compounds, TrpS has enjoyed only limited application (7). Optimized methods are restricted by low substrate concentrations and yields typically below 50% (7, 12, 13). To produce NCAAs, researchers have used the *S. typhimurium* TrpS complex (*St*TrpS), which suffers from poor thermostability and low tolerance to organic solvents (14). Although only the reactivity of the β-subunit, coupling of L-serine and indole, is necessary and desirable for synthetic applications, using TrpB as an isolated enzyme has not been feasible. Outside of its native complex, TrpB loses up to 95% of its native activity and is subject to inactivation (15, 16). These facts combine to present a compelling challenge: can we use directed evolution to recover the activity lost when TrpA is removed and create a highly active stand-alone TrpB enzyme? If so, what are the structural and kinetics effects of the mutations that harness this latent catalytic potential?

Significance

Many enzymes perform desirable biochemical transformations, but are not suitable to use as biocatalysts outside of the cell. In particular, enzymes from heteromeric complexes typically have decreased activity when removed from their protein partners. We used directed evolution to restore the catalytic efficiency of the tryptophan synthase β-subunit (TrpB), which synthesizes L-tryptophan from L-serine and indole, surpassing the activity of the native complex. Experiments show that activating mutations promote catalysis through the same mechanism as partner protein binding, establishing that isolated subunits may be readily reactivated through directed evolution. Engineering TrpB for stand-alone function restored high activity with indole analogs, providing a simplified enzyme platform for the biocatalytic production of noncanonical amino acids.

BIOCHEMISTRY

Fig. 1. Catalytic cycle of the native TrpS complex. (*A*) Indole (**4**) is released through a retro-aldol reaction in TrpA (red) and then diffuses through a 25-Å tunnel into TrpB (black), where a PLP-mediated β-substitution reaction occurs with ʟ-serine (**2**), yielding ʟ-tryptophan (**1**). The COMM domain is indicated in blue. Scheme is superimposed over *Pf*TrpS with Lys-PLP internal aldimine, E(Ain), shown in green sticks. The native complex is an αββα heterotetramer; a single αβ pair is shown for clarity. (*B*) Mechanism of ʟ-tryptophan formation. Transimination of ʟ-serine to form an external aldimine, E(Aex₁), followed by dehydration across $C_α$–$C_β$ through a quinonoid intermediate, E(Q₁), is designated stage I of the overall reaction. A mechanistically similar process occurs in reverse for the addition of indole into E(A-A) and subsequent release of ʟ-tryptophan, designated stage II of the reaction.

Results

Selection of the Parent Enzyme, TrpB, from *Pyrococcus furiosus*. We focused the search for an engineering starting point on known thermophilic TrpS enzymes for three reasons: (*i*) higher operating temperatures afford increased solubility of the hydrophobic substrates, which is useful for preparative reactions; (*ii*) thermostable enzymes are more tolerant to the introduction of activating but potentially destabilizing mutations (17); and (*iii*) thermostable enzyme variants can be screened efficiently (described below). We compared published kinetic properties of TrpS from *Thermotoga maritima* (18), *Thermococcus kodakaraensis* (19), and *Pyrococcus furiosus* (20–22) and selected the last for its superior kinetic parameters and thermostability (Table S1). In our hands, *Pf*TrpB heterologously expressed and purified from *E. coli* has a k_{cat} of 0.31 s⁻¹ and experiences a 12-fold increase in catalytic efficiency upon addition of purified *P. furiosus* TrpA (*Pf*TrpA) to make the *Pf*TrpS complex (Table 1), similar to values reported previously for *E. coli* TrpB (*Ec*TrpB) (15). Notably, *Pf*TrpB does not show the mechanism-based inactivation that inhibits use of *St*TrpB for preparation of NCAAs (23).

Directed Evolution of *Pf*TrpB for Stand-Alone Function. We performed random mutagenesis by error-prone PCR and screened a small *Pf*TrpB mutant library (528 clones) for increased V_{max} under saturating concentrations of substrate (ʟ-serine and indole). The extreme thermostability of the parent enzyme permitted a 1-h heat treatment of the lysates at high temperature (75 °C) that precipitated the majority of *E. coli* proteins and ensured that any activated variants retained significant stability. Formation of

ʟ-tryptophan took place at 75 °C for up to 1 h (generation 1, 1 h; generations 2 and 3, 6 min). The reactions were then quenched in an ice-water bath, and the production of ʟ-tryptophan was quantified at 290 nm with a plate reader. This procedure identified many activating mutations, with 3.8% (20/528) of the screened variants of generation 1 showing at least 40% greater product formation than the parent. A single mutation, T292S, gave rise to a 3.5-fold increase in k_{cat} compared with *Pf*TrpB, which completely recovered k_{cat} and even exceeded the catalytic efficiency (k_{cat}/K_M) of the *Pf*TrpS complex (Table 1). Twenty-six other mutations in 19 different variants also contributed activating effects (Fig. S1).

We recombined 12 of the most activating mutations identified in the first generation (*SI Materials and Methods*). Screening a total of 1,408 clones, we identified *Pf*TrpB⁴ᴰ¹¹ containing mutations E17G, I68V, F274S, T292S, and T321A. The k_{cat} of *Pf*TrpB⁴ᴰ¹¹ was 2.2 s⁻¹, a sevenfold improvement over wild type (Table 1). *Pf*TrpB⁴ᴰ¹¹ served as template for a final round of random mutagenesis, for which we screened 1,144 clones. *Pf*TrpB⁰ᴮ² carried one additional mutation, P12L, and had a k_{cat} that was 9.4-fold higher than *Pf*TrpB and threefold higher than *Pf*TrpS. With *Pf*TrpB⁰ᴮ² we had surpassed our goal of engineering an isolated enzyme domain to be as active as in its native complex.

Biochemical Comparison of Evolved *Pf*TrpB Enzymes with *Pf*TrpS. Kinetic analysis of *Pf*TrpB and *Pf*TrpS established that the 12-fold increase in the catalytic efficiency for indole upon complexation is driven by both an increase in k_{cat} and decrease in K_M (Table 1). Despite screening the mutant libraries under saturating

Table 1. Biochemical characterization of tryptophan synthases

Enzyme	Mutations	k_{cat}, s⁻¹	K_M, mM ʟ-serine	K_M, μM indole	k_{cat}/K_M, mM⁻¹s⁻¹ indole	k_{cat} change with TrpA*	T_{50} °C†
*Pf*TrpS	—	1.0	0.6	20	50	—	> 95
*Pf*TrpB	—	0.31	1.2	77	4	3.2	95
*Pf*TrpB²ᴳ⁹	**T292S**	1.1	0.84	14	78	0.34	95
*Pf*TrpB⁴ᴰ¹¹	**E17G, I68V**, T292S, **F274S, T321A**	2.2	1.2	11	200	0.3	84
*Pf*TrpB⁰ᴮ²	**P12L,** E17G, I68V, T292S, F274S, T321A	2.9	0.7	8.7	330	0.04	87

All kinetic data are measured at 75 °C using a previously described (15) continuous assay for Trp production. Additional mutations relative to their parent enzyme are highlighted in bold.
*The effect of *Pf*TrpA was measured by addition of a fivefold stoichiometric excess of *Pf*TrpA under conditions saturating in each substrate.
†T_{50} is the temperature of half-maximal activity after incubation for 1 h. Assay parameters are described in *Materials and Methods*. SE for each measurement is given in Table S2.
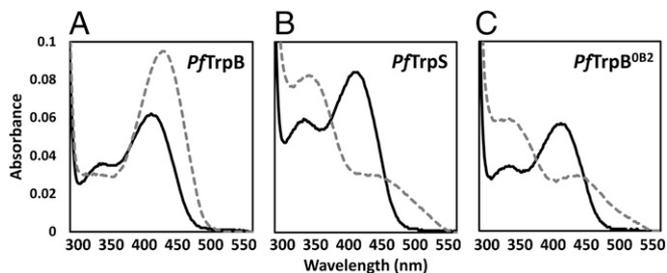
Fig. 2. UV-vis absorption spectra of native and engineered *Pf*TrpB. (*A*) The PLP absorption spectrum of *Pf*TrpB (black) has a $\lambda_{max} = 412$ nm, characteristic of E(Ain). Addition of 20 mM L-serine causes a red-shift to 428 nm (gray), consistent with E(Aex₁) formation. (*B*) Addition of L-serine to *Pf*TrpS causes a shift in λ_{max} to 350 nm, which is attributed to the E(A-A). A residual peak at 428 nm indicates population of E(Aex₁). (*C*) Like *Pf*TrpS, addition of 20 mM L-serine to *Pf*TrpB^OB2 shows $\lambda_{max} = 350$ nm as well as contributions from E(Aex₁). All spectra were collected with 20 μM of enzyme. See *Materials and Methods* for details.

conditions for both substrates, we observed a steady decrease in the K_M for indole in the enzymes with greater activity, which mimics the behavior of the native complex. The K_M for L-serine fluctuated during evolution, and in the final round the values for *Pf*TrpB^OB2 and *Pf*TrpS were similar.

Though Michaelis–Menten kinetic analysis provides a simple readout of overall catalytic performance, activity changes upon complex formation and during directed evolution are associated with a shift in the populations of the intermediates in the TrpB catalytic cycle. The PLP cofactor absorbs in the UV-vis region, and different chemical intermediates have characteristic peaks that can be measured readily (Fig. 1*B*). Under turnover conditions, the recorded spectrum reflects the Boltzmann-weighted average of each of the intermediates in the catalytic cycle. Incubation of *Pf*TrpB with L-serine results in a large increase in absorption at 428 nm, consistent with accumulation of E(Aex₁) (Fig. 2*A*). A peak at 320 nm developed over several minutes, whereas the absorption at 428 nm remained constant (Fig. S2), which we attribute to the previously characterized serine deaminase activity that is an artifact of not having a competing nucleophile present (24). In contrast, L-serine-bound *Pf*TrpS has a λ_{max} near 350 nm, consistent with a shift in the equilibrium to populate the E(A-A) (Fig. 2*B*) (2). With the engineered proteins, the external aldimine absorbance at 428 nm decreases, and the absorbance bands at 350 nm grow in intensity over the course of directed evolution of Trp synthase activity (Fig. 2*C* and Fig. S2).

One question motivating this study was how mutational reactivation alters the allosteric regulation of *Pf*TrpB by its TrpA protein partner. Adding purified *Pf*TrpA to each TrpB variant gave a surprising result: instead of enhancing activity (or doing nothing), *Pf*TrpA inhibited each improved TrpB, an effect that was stronger with each evolutionary step, to the point where *Pf*TrpB^OB2 had just 4% of its activity when *Pf*TrpA was added (Table 1).

Structural Analysis of *Pf*TrpB. Whereas the residues that perform the TrpB chemistry are conserved throughout evolution, the conformational motions associated with allosteric signaling have not been characterized outside of *St*TrpS or in the absence of the α-subunit. We obtained high-resolution structures of wild-type *Pf*TrpB in its ligand-free state, bound to its L-serine substrate, and bound to its L-tryptophan product (Table S3). Comparison of the ligand-free and Ser-bound structures (at 1.69 Å and 2.0 Å resolution, respectively) reveals motion of the COMM domain into a partially closed state upon serine binding, as well as a hydrogen bond between Asp300 and the Ser-hydroxyl of E(Aex₁) (Fig. 3 *A* and *B*). This large conformational rearrangement is structurally equivalent to that characterized for *St*TrpS (25), with 0.5 Å rmsd between the E(Aex₁) forms of TrpB (Fig. S3), despite the modest (59%) sequence identity and lack of an α-subunit. Combined with their similar biochemical properties, this structural

conservation constitutes firm experimental support for applying insights gleaned from *St*TrpS and *Ec*TrpS to the function of *Pf*TrpB. Labeling studies have shown that β-substitution occurs with retention of stereochemistry, indicating the hydroxyl of E(Aex₁) must rotate 180° from its crystallographically observed state to eliminate from the same face to which indole is added (26). The H-bond between E(Aex₁) and Asp300 is, therefore, transient during the catalytic cycle and suggests an important role for the H-bond between Thr292 and Asp300 that we observed in the ligand-free structure. Notably, T292S was one of the most activating mutations identified in the first round of directed evolution (Fig. 4 *A* and *B* and Table 1). When L-Ser is incubated with *Pf*TrpB^2G9, the UV-vis spectrum clearly shows that the equilibrium is shifted toward E(A-A) (Fig. S2*B*). We hypothesize that this mutation alters the energetics of the Asp300-E(Aex₁) interaction to favor the fully closed conformational state of the enzyme and thereby accelerate the reaction.

The structure of *Pf*TrpB with L-tryptophan bound in the active site at 1.74 Å resolution shows the product is not covalently linked to the PLP cofactor, but is in a novel ligand-binding pose (Fig. 3*C*). Residues Thr105 to His110 comprise a carboxylate binding motif (4) that we report also forms H-bonds to the primary amine of L-tryptophan through the backbone N–H of Ala106. This same residue also H-bonds with the Ser-hydroxyl of E(Aex₁). Asp300, however, is not observed to interact with L-tryptophan. A hydrogen bond between Glu104 and the N-1 of L-tryptophan likely also occurs when indole binds. This interaction may serve to increase the nucleophilicity of indole by positioning C-3 close to the acrylate of E(A-A) and by increasing electron density of the arene (Fig. 1*B*) (2, 4). Glu104 is located in the COMM domain and shifts closer to the active site upon closure (Fig. 3*A*). In each of the substrate- and product-bound structures, we observed a rotameric shift of Phe274 and His275 (Fig. 4*C*) that may function as a gate within the indole tunnel (Fig. 4*D*). In the structure of *Pf*TrpS, we observe a hydrogen bond between His275 and Asp43 from the α-subunit, indicating that *Pf*TrpA binding stabilizes this open conformation (Fig. S4*A*). In *St*TrpS, NMR analysis has shown this motion is concerted, and our observation that it is conserved across species is consistent with it having an important role for regulating catalytic function (27). The location of the F274S mutation is therefore quite striking, because it may alter the energetics of this transition to favor higher activity.

Two mutations, E17G and P12L, map onto the α/β interface of a previously determined 3.0-Å structure of *Pf*TrpS (22), but this low resolution precluded confident assessment of the side-chain interactions for these residues. We solved a higher-resolution
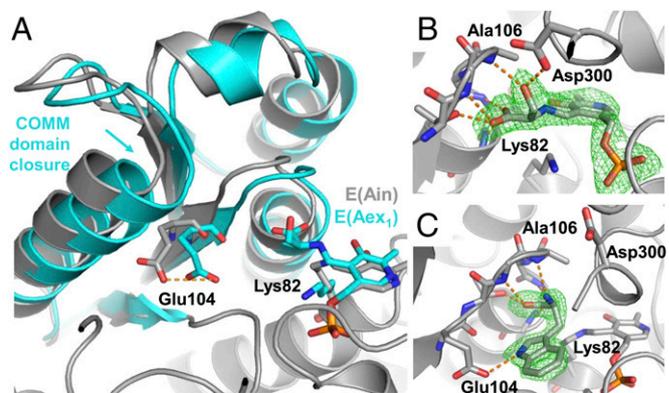
Fig. 3. Structural transitions upon ligand binding in *Pf*TrpB. (*A*) Superimposition of *Pf*TrpB-E(Ain) and *Pf*TrpB-E(Aex₁) in gray and cyan, respectively. Overlay shows the 2.1-Å displacement of the COMM domain upon E(Aex₁) formation. This closure moves the side chain of Glu104 by 3.7 Å, toward its catalytic orientation (orange dashes). (*B*) Structure of Ser-bound *Pf*TrpB with a Fₒ–F𝒸 map of E(Aex₁) contoured at 3.0 σ (green). (*C*) Structure of L-tryptophan–bound *Pf*TrpB with Fₒ–F𝒸 map of Trp ligand contoured at 3.0 σ.
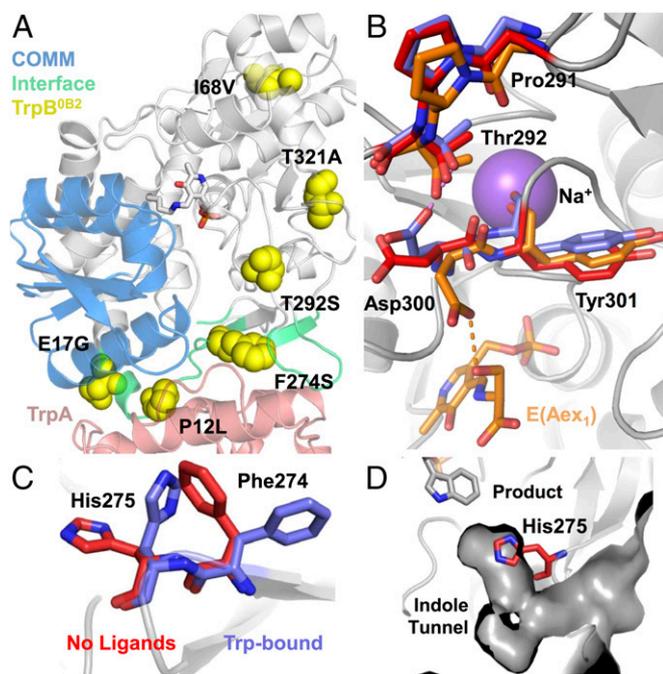
Fig. 4. Distribution of *Pf*TrpB^OB2 mutations and interaction networks altered by mutational reactivation. (*A*) *Pf*TrpB residues within 5 Å of *Pf*TrpA (red) are colored cyan and the COMM domain is colored blue. (*B*) A hydrogen bond between D300 and E(Aex₁) in the Ser-bound structure (orange) is formed transiently during the catalytic cycle. When this H-bond is severed, D300 may interact with T292 (no ligands, red, or Trp-bound, blue). This complex network is centered on a monovalent cation cofactor, shown here as Na⁺, which is known to mediate allosteric interactions between the α- and β-subunits (6). (*C*) Residues F274 and H275 undergo a rotameric shift upon substrate or product binding into an open state (blue). (*D*) In the closed state (red, no ligands bound), H275 blocks access to the active site.

structure at 2.76 Å that revealed a salt bridge between Glu17 of *Pf*TrpB and Arg148 of *Pf*TrpA (Fig. S4*B*). Pro12 of *Pf*TrpB is an evolutionarily conserved residue that lies along the indole tunnel between the two subunits, where previous studies have found that mutation to bulkier residues inhibits substrate channeling (28). Such interactions are clearly disrupted at the α/β interface (Fig. S4*C*), but the strong inhibition of *Pf*TrpB^OB2 upon *Pf*TrpA addition demonstrates that these proteins still associate. Finally, two mutations present in *Pf*TrpB^OB2, I68V and T321A, are distal to sites that undergo an observable structural change upon substrate binding or complex formation, and their contribution to rate enhancement is difficult to rationalize. Overall, 60% of the activating mutations identified through random mutagenesis were located within 5 Å of the α/β interface, the COMM domain, or regions that undergo observable motion upon transition to the closed conformation (Fig. S1). These positions comprise just 31% of the protein sequence, indicating modest enrichment within residues in the immediate spatial route between the α/β interface and the β-subunit active site. In contrast to the many mutations that have been identified as deleterious to the allosteric communication in TrpS (29, 30), the mutations identified here using directed evolution are the first reported to affect allosteric communication and increase the activity of TrpB in isolation.

PfTrpB^OB2 Is a Stand-Alone Catalyst for Production of NCAAs. Our selection of TrpB to evolve for high activity outside of its native complex was motivated by practical considerations. Previous studies have shown that *St*TrpS is a promiscuous enzyme, capable of synthesizing diverse analogs of L-tryptophan (7, 13). These analogs require subtly different transition state stabilization for catalysis, but the role of allostery in promoting this desirable chemistry has not been studied. We selected a representative

panel of substrate analogs to study promiscuous activity in the native and engineered proteins (Fig. 5*A*). The *St*TrpS complex reacts with most halogenated and methylated indoles, which only modestly change the steric and electronic properties of the indole ring and afford reactivity at C3. Alternatively, indazole (**5**) and indoline (**6**), which have substantially altered electronic properties, react at N1 for C–N bond formation. We measured the relative rate of *Pf*TrpB compared with *Pf*TrpS and observed much larger rate enhancements for TrpB on the indole derivatives than on the native substrate (Fig. 5*B*), up to a 100-fold increase in the rate of NCAA synthesis with 5-bromoindole (**7**). These results raised an important question about our objective to engineer *Pf*TrpB for function as an independent subunit by directed evolution: will screening for higher activity with indole translate into increased activity on alternative substrates, or will evolution generate an enzyme that is highly active on indole but less active toward other substrates, as has been observed in directed evolution of other enzymes (31, 32)?

We measured the activity of *Pf*TrpB^OB2 on the substrate panel (Fig. 5*B*) and were pleased to observe a substantial increase in activity relative to *Pf*TrpB for all nucleophiles tested. The activity profile is broadly similar to that of *Pf*TrpS, with a few exceptions. The *Pf*TrpS complex reacts approximately eightfold faster than *Pf*TrpB^OB2 with bromoindole **7**, whereas *Pf*TrpB^OB2 reacts approximately sixfold faster than *Pf*TrpS with indoline **6** and threefold faster with indazole **5**. The identity of each product was confirmed by mass spectrometry and NMR in reactions using *Pf*TrpB^OB2. Because we screened for increases in V_{max} during laboratory evolution, the variants we selected also have improved expression levels relative to *Pf*TrpB. *E. coli* cultures produce threefold more soluble and active *Pf*TrpB^OB2 than *Pf*TrpB, exceeding 230 mg enzyme per liter culture, facilitating preparative reactions and future use of *Pf*TrpB^OB2 as a biocatalyst.

Discussion

We evolved *Pf*TrpB for independent function by selecting mutations that increased its V_{max} in heat-treated *E. coli* lysates. We found that activating mutations were unusually common, which could in part be attributed to the high thermal stability of the parent enzyme that increases tolerance to the introduction of random mutations (17). However, it is clear that many mutations have the potential to recover activity lost when TrpB is removed from its native complex. The single T292S mutation raised the catalytic efficiency of *Pf*TrpB on indole by almost 20-fold and completely restored activity to TrpS-like levels (Table 1). Further evolution resulted in the identification of *Pf*TrpB^OB2, which retained T292S as well as five additional mutations. This variant has an 83-fold increase in catalytic efficiency on indole compared with *Pf*TrpB. The T292S and F274S mutations occur in dynamic regions of TrpB related to catalytic function, as discussed above. However, the majority of the mutations in *Pf*TrpB^OB2, and 40%
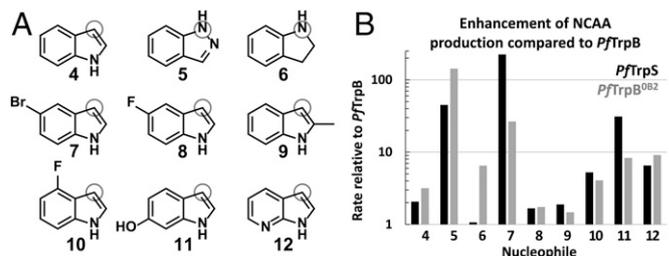
Fig. 5. Substrate profile of native and engineered TrpB enzymes. (*A*) Indole analogs that have been reported to react with *St*TrpS were tested for reactivity with the *Pf*TrpB, *Pf*TrpS, and *Pf*TrpB^OB2 enzymes. The nucleophilic atom is indicated with a gray circle. (*B*) Relative activities of enzyme complex *Pf*TrpS (black) and *Pf*TrpB^OB2 (gray) compared with *Pf*TrpB. Reactions performed in duplicate with 20 mM of each substrate and varying enzyme concentrations to ensure incomplete conversion after 1 h. Products were later confirmed in scaled-up reactions using *Pf*TrpB^OB2. See *Materials and Methods* for details.

of all activating mutations that we identified, are at positions that do not undergo any observable structural changes upon formation of the partially closed state, nor do the corresponding residues in *St*TrpS move upon formation of the fully closed state (2). The location of many activating mutations outside of any observed allosteric site raises the central question of this study: did directed evolution increase activity through the same mechanism(s) through which TrpA binding regulates function? If so, we posit that increases in k_{cat}, which was under selective pressure during directed evolution, would be coupled to other kinetic and spectroscopic characteristics of the native complex for which there was no selective pressure.

To a first approximation, the open–close equilibrium of TrpB can be inferred from its K_M for indole because TrpA binding stabilizes the closed conformation (2) and decreases the K_M (Table 1). Each generation of evolution of *Pf*TrpB produced a lower K_M for indole, to values below those in *Pf*TrpS, despite screening under saturating conditions (Table 1). UV-vis spectroscopy affords a more-sensitive probe of the active site environment because the steady-state distribution of intermediates in the catalytic cycle can be directly observed. Measurement of the steady-state population of the stage I intermediates in *Pf*TrpB shows that the electrophilic E(A-A) state is stabilized relative to E(Aex$_1$) when *Pf*TrpA binds. This same stabilization of E(A-A) is observed in TrpB enzymes evolved for independent function (Fig. 2). These data reflect the properties of *Pf*TrpB in its native reaction. Activity on indole analogs is also significantly increased by *Pf*TrpA binding, with the rate enhancements differing by two orders of magnitude between diverse indole analogs (Fig. 5). Because each of these substrates requires slightly different transition state stabilization, the rate enhancement upon effector addition is a sensitive metric for changes in the conformational ensemble that are relevant to catalysis. Consistent with the data measured on the native reaction, we observed that increases in activity with indole analogs caused by mutation were similar to the effects of TrpA addition (Fig. 5). Taken together, these data support the hypothesis that increases in *Pf*TrpB activity from directed evolution arose through the same mechanism by which effector binding activates catalysis.

A perplexing observation about mutational reactivation is that addition of *Pf*TrpA to the engineered proteins did not result in allosteric activation, but instead inhibited catalysis. A simple open–closed model of the ensemble might imply that TrpA binding and mutations that stabilize the closed state would be additive in their effects on catalysis. Though the introduction of mutations may change the nature of the allosteric signaling that results from TrpA binding, no such assumption is required to explain the inhibition. It is well documented that stabilization of the closed state by effector binding alters the energetics of multiple transition states of TrpB (2). These changes in transition-state energy result in a lower overall barrier to the reaction. Doubling these energetic perturbations (e.g., TrpA and the mutations combined) would lower the energy of the original rate-limiting step, but could end up impeding catalysis by increasing the energy of a different step above the original reaction barrier (Fig. S5). With this explanation, the inhibitory effect of TrpA becomes consistent with the demonstration that the mutations and effector addition accelerate catalysis through the same mechanism.

Allostery is common in enzymes and has been targeted in previous protein engineering endeavors (*vide infra*). To compare the role of allostery in these diverse efforts, we define the change in activity that arises through effector binding as an enzyme's allosteric potential. In this view, it has been shown that allosteric potential can be decreased by using mutagenesis to disrupt specific interactions between fructose-1,6-bisphosphatase and its effector, adenosine monophosphate (33). Recent studies have also shown that engineering can increase allosteric potential, enhancing inhibition of phosphofructokinase by phosphoenol-pyruvate (34). An allosteric potential can even be engineered into enzymes where previously one did not exist (35). Nature has found mutations that constitutively activate allosterically regulated

enzymes, as is well known in phosphorylation cascades contributing to tumorigenesis (36). Finding such mutations for engineering purposes has proved challenging. The native substrate of the acyl-transferase LovD is covalently bound to an acyl carrier protein, LovF, which also functions as an allosteric activator. LovD was subjected to nine rounds of directed evolution for altered substrate specificity, thermal stability, and tolerance to organic solvent to generate a biocatalyst for production of the drug simvastatin (37). Insight into whether increases in activity were related to allosteric regulation was gleaned from microsecond molecular dynamics simulations, which suggested that LovF promotes the stability of a closed and catalytically active conformation of LovD and that directed evolution identified mutations that increased activity in a similar fashion (37). Our kinetic, structural, and spectroscopic data provide firm experimental support for a similar effect in TrpB, demonstrating that allosteric potential can be readily converted into catalytic activity through directed evolution.

We advocate that future efforts to recoup allosteric potential not be limited to making mutations within a hypothetical allosteric pathway (38). Residues whose interactions are not changed upon effector addition can nonetheless tune the cooperative network of interactions that transfer allosteric signals (39). More generally, allostery enables proteins to respond to environmental cues, and often only small energetic differences separate active conformations from inactive or less-active ones. The protein ensembles of such enzymes are likely to be sensitive to the effects of widely distributed mutations. Indeed, a single conservative mutation (T292S) was sufficient to raise the catalytic efficiency of *Pf*TrpB to the level of the TrpS complex, and many other mutations contributed smaller activating effects. Therefore, we anticipate that recovering allosteric potential with directed evolution will be broadly achievable.

These insights into the modulation of protein allosteric regulation are of both fundamental and practical interest. Our observation that the activity of *Pf*TrpB was enhanced on a range of substrates is consistent with the hypothesis that the mutations alter transition-state stabilization in a manner similar to *Pf*TrpA binding; it also establishes a greatly simplified enzyme platform for production of NCAAs. This demonstration that isolated subunits may be readily reactivated through directed evolution provides a useful tool for the chemical biology community and expands the scope of enzymes accessible for biocatalysis.

Materials and Methods

Detailed experimental methods are presented in *SI Materials and Methods*.

Cloning, Expression, and Purification of *Pf*TrpA and *Pf*TrpB. The genes encoding *Pf*TrpB (UNIPROT ID Q8U093) and *Pf*TrpA (UNIPROT ID Q8U094) were obtained as gBlocks and cloned into pET22(b)+ for expression in *E. coli* BL21 *E. cloni* EXPRESS cells (Lucigen). Heterologous protein expression of *Pf*TrpA and *Pf*TrpB was performed in Terrific Broth with 100 μg/mL ampicillin (TB$_{amp}$) and induced with 500 mM IPTG (final concentration 1 mM). *Pf*TrpB was purified via a HisTrap HP column. *Pf*TrpA was purified via a Q HP HiTrap column (flow-through), followed by ammonium sulfate precipitation, and hydrophobic interaction chromatography on a phenyl Sepharose HP HiTrap column (Fig. S6).

Library Construction and High-Throughput Screening. Error-prone PCR libraries were constructed using standard protocols with either MnCl$_2$ or Mutazyme II (Stratagene). DNA shuffling and site-directed mutagenesis by overlap extension (SOE) PCR were performed to recombine activating mutations. The resulting libraries were cloned into pET22(b)+ with the C-terminal his-tag for expression in *E. coli* BL21 *E. cloni* EXPRESS cells. High-throughput expression and screening were performed on 96-well scale. Formation of L-tryptophan was recorded at 290 nm.

Kinetics and UV-Vis Spectroscopy. Data were collected between 550 and 250 nm on a UV1800 Shimadzu spectrophotometer (Shimadzu) using 0.25–20 μM of enzyme in 200 mM potassium phosphate (pH 8.0) in a quartz cuvette. Samples were incubated at 75 °C for >3 min to ensure a stable temperature was reached. *Pf*TrpB activity (k_{cat}) was measured by monitoring tryptophan formation at 290 nm using $\Delta\varepsilon_{290} = 1.89$ mM^{-1}·cm^{-1} (15).

Substrate Selectivity. The relative rate of NCAA production was measured using 20 mM L-serine and 20 mM indole analog (Fig. 5A) in 200 mM potassium phosphate (pH 8.0) with 5% (vol/vol) DMSO. Reactions were incubated at 75 °C for 1 h, quenched, and the relative rate of production formation was measured by comparing the ratio of the product peaks measured via ultra HPLC-MS (UHPLC-MS) Agilent 1290 with 6140 MS detector at 280 nm and then normalizing for the enzyme concentration.

Crystallography. Crystals of *Pf*TrpB and *Pf*TrpS were grown using the sitting-drop vapor diffusion method, and cryoprotected before diffraction at the Stanford Synchrotron Radiation Laboratories on beamline 12-2. Ligand-bound crystals of *Pf*TrpB were prepared by soaking preformed crystals with a concentrated solution of L-Ser or L-Trp. Structures were determined by molecular replacement and models were built using standard procedures.

Identification of Nonnatural Amino Acid Products. Preparative-scale reactions were conducted using *Pf*TrpB^{0B2}, which was prepared as a heat-treated lysate. Products were purified directly on C-18 silica, and their identities confirmed by ^{1}H NMR and low-resolution mass spectrometry (LRMS). The optical purity of the products was estimated by derivatization with *N*-(5-fluoro-2, 4-dinitrophenyl)alanamide (FDNP-alanamide).

1. Du L, Lou L (2010) PKS and NRPS release mechanisms. *Nat Prod Rep* 27(2):255–278.
2. Dunn MF (2012) Allosteric regulation of substrate channeling and catalysis in the tryptophan synthase bienzyme complex. *Arch Biochem Biophys* 519(2):154–166.
3. Davidsen JM, Bartley DM, Townsend CA (2013) Non-ribosomal propeptide precursor in nocardicin A biosynthesis predicted from adenylation domain specificity dependent on the MbtH family protein NocI. *J Am Chem Soc* 135(5):1749–1759.
4. Niks D, et al. (2013) Allostery and substrate channeling in the tryptophan synthase bienzyme complex: Evidence for two subunit conformations and four quaternary states. *Biochemistry* 52(37):6396–6411.
5. Hyde CC, Ahmed SA, Padlan EA, Miles EW, Davies DR (1988) Three-dimensional structure of the tryptophan synthase alpha 2 beta 2 multienzyme complex from *Salmonella typhimurium*. *J Biol Chem* 263(33):17857–17871.
6. Dierkers AT, Niks D, Schlichting I, Dunn MF (2009) Tryptophan synthase: Structure and function of the monovalent cation site. *Biochemistry* 48(46):10997–11010.
7. Phillips RS (2004) Synthetic applications of tryptophan synthase. *Tetrahedron Asymmetry* 15(18):2787–2792.
8. Lang K, Chin JW (2014) Cellular incorporation of unnatural amino acids and bio-orthogonal labeling of proteins. *Chem Rev* 114(9):4764–4806.
9. Barry SM, et al. (2012) Cytochrome P450–catalyzed L-tryptophan nitration in thaxtomin phytotoxin biosynthesis. *Nat Chem Biol* 8(10):814–816.
10. Kieffer ME, Repka LM, Reisman SE (2012) Enantioselective synthesis of tryptophan derivatives by a tandem Friedel-Crafts conjugate addition/asymmetric protonation reaction. *J Am Chem Soc* 134(11):5131–5137.
11. Patel RN (2013) Biocatalytic synthesis of chiral alcohols and amino acids for development of pharmaceuticals. *Biomolecules* 3(4):741–777.
12. Smith DRM, et al. (2014) The first one-pot synthesis of L-7-iodotryptophan from 7-iodoindole and serine, and an improved synthesis of other L-7-halotryptophans. *Org Lett* 16(10):2622–2625.
13. Goss RJM, Newill PLA (2006) A convenient enzymatic synthesis of L-halotryptophans. *Chem Comm* 47:4924–4925.
14. Ahmed SA, Miles EW (1994) Aliphatic alcohols stabilize an alternative conformation of the tryptophan synthase alpha 2 beta 2 complex from *Salmonella typhimurium*. *J Biol Chem* 269(23):16486–16492.
15. Lane AN, Kirschner K (1983) The catalytic mechanism of tryptophan synthase from *Escherichia coli*. Kinetics of the reaction of indole with the enzyme–L-serine complexes. *Eur J Biochem* 129(3):571–582.
16. Lane AN, Kirschner K (1983) The mechanism of binding of L-serine to tryptophan synthase from *Escherichia coli*. *Eur J Biochem* 129(3):561–570.
17. Bloom JD, Labthavikul ST, Otey CR, Arnold FH (2006) Protein stability promotes evolvability. *Proc Natl Acad Sci USA* 103(15):5869–5874.
18. Hettwer S, Sterner R (2002) A novel tryptophan synthase beta-subunit from the hyperthermophile *Thermotoga maritima*. Quaternary structure, steady-state kinetics, and putative physiological role. *J Biol Chem* 277(10):8194–8201.
19. Hiyama T, Sato T, Imanaka T, Atomi H (2014) The tryptophan synthase β-subunit paralogs TrpB1 and TrpB2 in *Thermococcus kodakarensis* are both involved in tryptophan biosynthesis and indole salvage. *FEBS J* 281(14):3113–3125.
20. Yamagata Y, et al. (2001) Entropic stabilization of the tryptophan synthase alpha-subunit from a hyperthermophile, *Pyrococcus furiosus*. X-ray analysis and calorimetry. *J Biol Chem* 276(14):11062–11071.
21. Hioki Y, et al. (2004) The crystal structure of the tryptophan synthase beta subunit from the hyperthermophile *Pyrococcus furiosus*. Investigation of stabilization factors. *Eur J Biochem* 271(13):2624–2635.
22. Lee SJ, et al. (2005) Conformational changes in the tryptophan synthase from a hyperthermophile upon alpha2beta2 complex formation: Crystal structure of the complex. *Biochemistry* 44(34):11417–11427.
23. Ahmed SA, Ruvinov SB, Kayastha AM, Miles EW (1991) Mechanism of mutual activation of the tryptophan synthase alpha and beta subunits. Analysis of the reaction specificity and substrate-induced inactivation of active site and tunnel mutants of the beta subunit. *J Biol Chem* 266(32):21548–21557.
24. Miles EW, McPhie P (1974) Evidence for a rate-determining proton abstraction in the serine deaminase reaction of the beta 2 subunit of tryptophan synthetase. *J Biol Chem* 249(9):2852–2857.
25. Ngo H, et al. (2007) Allosteric regulation of substrate channeling in tryptophan synthase: Modulation of the L-serine reaction in stage I of the beta-reaction by alpha-site ligands. *Biochemistry* 46(26):7740–7753.
26. Miles EW, Houck DR, Floss HG (1982) Stereochemistry of sodium borohydride reduction of tryptophan synthase of *Escherichia coli* and its amino acid Schiff's bases. *J Biol Chem* 257(23):14203–14210.
27. McDowell LM, Lee M, McKay RA, Anderson KS, Schaefer J (1996) Intersubunit communication in tryptophan synthase by carbon-13 and fluorine-19 REDOR NMR. *Biochemistry* 35(10):3328–3334.
28. Schlichting I, Yang XJ, Miles EW, Kim AY, Anderson KS (1994) Structural and kinetic analysis of a channel-impaired mutant of tryptophan synthase. *J Biol Chem* 269(43):26591–26593.
29. Rowlett R, et al. (1998) Mutations in the contact region between the alpha and beta subunits of tryptophan synthase alter subunit interaction and intersubunit communication. *Biochemistry* 37(9):2961–2968.
30. Raboni S, Bettati S, Mozzarelli A (2005) Identification of the geometric requirements for allosteric communication between the alpha- and beta-subunits of tryptophan synthase. *J Biol Chem* 280(14):13450–13456.
31. Aharoni A, et al. (2005) The 'evolvability' of promiscuous protein functions. *Nat Genet* 37(1):73–76.
32. Bloom JD, Romero PA, Lu Z, Arnold FH (2007) Neutral genetic drift can alter promiscuous protein functions, potentially aiding functional evolution. *Biol Direct* 2:17.
33. Yang J-S, Seo SW, Jang S, Jung GY, Kim S (2012) Rational engineering of enzyme allosteric regulation through sequence evolution analysis. *PLOS Comput Biol* 8(7):e1002612.
34. McGresham MS, Reinhart GD (2015) Enhancing allosteric inhibition in *Thermus thermophilus* Phosphofructokinase. *Biochemistry* 54(3):952–958.
35. Lee J, et al. (2008) Surface sites for engineering allosteric control in proteins. *Science* 322(5900):438–442.
36. Torkamani A, Verkhivker G, Schork NJ (2009) Cancer driver mutations in protein kinase genes. *Cancer Lett* 281(2):117–127.
37. Jiménez-Osés G, et al. (2014) The role of distant mutations and allosteric regulation on LovD active site dynamics. *Nat Chem Biol* 10(6):431–436.
38. Reynolds KA, McLaughlin RN, Ranganathan R (2011) Hot spots for allosteric regulation on protein surfaces. *Cell* 147(7):1564–1575.
39. Hilser VJ, Dowdy D, Oas TG, Freire E (1998) The structural distribution of cooperative interactions in proteins: Analysis of the native state ensemble. *Proc Natl Acad Sci USA* 95(17):9903–9908.
40. Gibson DG, et al. (2009) Enzymatic assembly of DNA molecules up to several hundred kilobases. *Nat Methods* 6(5):343–345.
41. Stemmer WPC (1994) DNA shuffling by random fragmentation and reassembly: In vitro recombination for molecular evolution. *Proc Natl Acad Sci USA* 91(22):10747–10751.
42. Kunkel TA, Roberts JD, Zakour RA (1987) Rapid and efficient site-specific mutagenesis without phenotypic selection. *Methods Enzymol* 154:367–382.
43. Kabsch W (2010) XDS. *Acta Crystallogr D Biol Crystallogr* 66(Pt 2):125–132.
44. Evans PR, Murshudov GN (2013) How good are my data and what is the resolution? *Acta Crystallogr D Biol Crystallogr* 69(Pt 7):1204–1214.
45. Karplus PA, Diederichs K (2012) Linking crystallographic model and data quality. *Science* 336(6084):1030–1033.
46. McCoy AJ, et al. (2007) Phaser crystallographic software. *J Appl Cryst* 40(Pt 4):658–674.
47. Winn MD, et al. (2011) Overview of the CCP4 suite and current developments. *Acta Crystallogr D Biol Crystallogr* 67(Pt 4):235–242.
48. Emsley P, Cowtan K (2004) Coot: Model-building tools for molecular graphics. *Acta Crystallogr D Biol Crystallogr* 60(Pt 12 Pt 1):2126–2132.
49. Winn MD, Murshudov GN, Papiz MZ (2003) Macromolecular TLS refinement in REFMAC at moderate resolutions. *Methods Enzymol* 374:300–321.
50. Chen VB, et al. (2010) MolProbity: All-atom structure validation for macromolecular crystallography. *Acta Crystallogr D Biol Crystallogr* 66(Pt 1):12–21.